Performance Characteristics of Frisch-Ring CdZnTe Detectors

A. E. Bolotnikov, *Member, IEEE*, G. C. Camarda, G. A. Carini, *Member, IEEE*, M. Fiederle, L. Li, D. S. McGregor, W. McNeil, G. W. Wright, and R. B. James, *Fellow, IEEE*

***Abstract*—The performance characteristics of Frisch-ring CdZnTe (CZT) detectors are described and compared with other types of CZT devices. The Frisch-ring detector is a bar-shaped CZT crystal with a geometrical aspect ratio of $\sim 1:2$. The side surfaces of the detector are coated with an insulating layer followed by a metal layer deposited directly upon the insulator. The simple design operates as a single-carrier device. Despite the simplicity of this approach, its performance depends on many factors that are still not fully understood. We describe results of testing several detectors fabricated from CZT material produced by different vendors and compare the results with numerical simulations of these devices.**

***Index Terms*—CdZnTe, detectors, Frisch-ring, room-temperature semiconductor detectors, virtual Frisch-grid.**

I. Introduction

SEMI-INSULATING CdZnTe (CZT) has great potential in ambient temperature gamma ray semiconductor detector applications [1]. However, the currently available CZT crystals are small, typically less than $15 \times 15 \times 10$ mm^3, which means that discrete elements have to be used to assemble arrays or stacks in order to produce large area/volume detectors. The second problem is related to the fact that CZT detectors are single-charge-carrier devices. To overcome the deleterious effects of uncollected holes upon energy resolution, special detector designs have to be implemented. For example, the small pixel effect device, the co-planar grid device, and the virtual Frisch-grid device [2].

The Frisch-ring devices have been successfully used for large thickness (>6 mm) but small area ($<5 \times 5$ mm^2) CZT crystals. These devices are designed to mimic the charge shielding effect in classical gas ionization chambers [3]. The first such semiconductor detector was introduced as a simple semiconductor bar with side conductive strips acting as the Frisch grid [4]. A variety of similar designs have been proposed and tested [5], [6], including a concept of the capacitive Frisch-grid device [7]. In this design, the shielding electrodes are separated from the crystal surface by a thin layer of dielectric material and cover the entire region between the anode and cathode electrodes. The shielding electrodes can be kept either at the ground or the cathode potentials. A unique aspect of the noncontacting Frisch-ring device is the simplicity, yet the spectral performance can be outstanding. The shape of these devices makes them ideal building blocks for assembling large arrays, which can provide a large effective area, good energy resolution, and good spatial resolution at comparatively low production cost.

The goal of the present effort is to develop an array of Frisch-ring CZT detectors for gamma-ray imaging and spectroscopy. Previous reported results from prototype virtual Frisch-grid devices demonstrated the energy resolution of $<1.5\%$ FWHM at 662 keV [8], [9]. However, it was observed that the detectors, when re-fabricated from the same CZT crystal, had wide variations in performance (from poor to good), thereby demonstrating the importance of the sample preparation and fabrication procedure. Specifically, we think that these variations can be attributed to the CZT side surface effect on the drift field inside the detector [9]. New results that support this supposition are presented in this paper.

II. Experimental Setup

The commercial CZT samples, acquired from eV-Products, Yinnel Tech Inc., and Saint-Gobain, were re-shaped into bar detectors with different geometrical aspect ratios: the detector width-to-length (W/L) ratio. Fabrication of the bar-shaped CZT detectors was conducted as previously described [8], [9]. The original crystals were hand polished and etched briefly with a 2% bromine/methanol solution. Electroless Au contacts were applied only to the ends, thereby forming the anode and cathode contacts. Afterwards, the side surfaces were polished further to reduce side-surface leakage current. To improve the device performance, the side surfaces of some of the samples were treated with a NH_4F/H_2O_2 solution [10].

A schematic design of the virtual Frisch-grid devices investigated in this work is shown in Fig. 1. After the bar-shaped crystals were fabricated, their side surfaces were wrapped in Teflon tape followed by Cu tape. During the measurements, the detector under test was placed inside a standard eV-Products device holder [9] or a custom-made test box. In the first case, the cathode and shielding electrodes were grounded, while a

Manuscript received March 10, 2005; revised May 30, 2005. This work was supported in part by the U.S. Department of Energy, Office of Nonproliferation Research and Engineering, NA-22. This work has been authored by Brookhaven Science Associates, LLC under Contract no. DE-AC02-98CH1-886 with the U.S. Department of Energy. The United States Government retains, and the publisher, by accepting the article for publication, acknowledges, a world-wide license to publish or reproduce the published form of this manuscript, or allow others to do so, for United States Government purposes

A. E. Bolotnikov, G. C. Camarda, G. A. Carini, and R. B. James are with Brookhaven National Laboratory, Upton, NY 11793 USA (e-mail: bolotnik@bnl.gov).

M. Fiederle is with Freiburger Materialforschungszentrum (FMF), Albert-Ludwigs-Universitaet Freiburg, Freiburg D-79104, Germany.

G. W. Wright is with Oak Ridge National Laboratory, Oak Ridge, TN 37831 USA.

L. Li is with Yinnel Tech, Inc., South Bend, IN 46619 USA.

D. S. McGregor and W. McNeil are with Kansas State University, Manhattan, KS 66506 USA.

Digital Object Identifier 10.1109/TNS.2006.871509

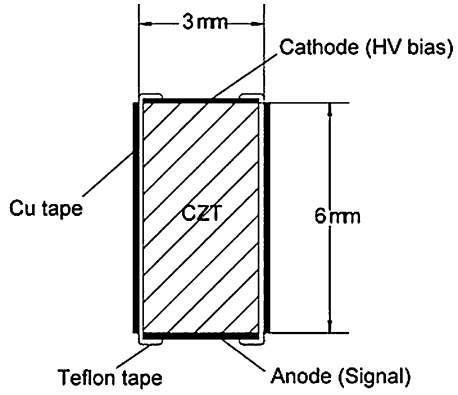

Fig. 1. Schematic of the Frisch-ring device.

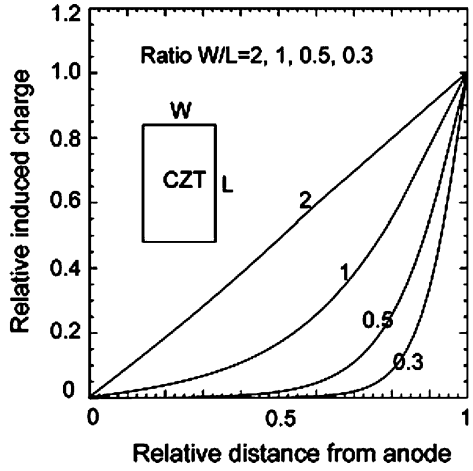

Fig. 2. Dependence of the induced charge versus the distance from the anode calculated for different aspect ratios.

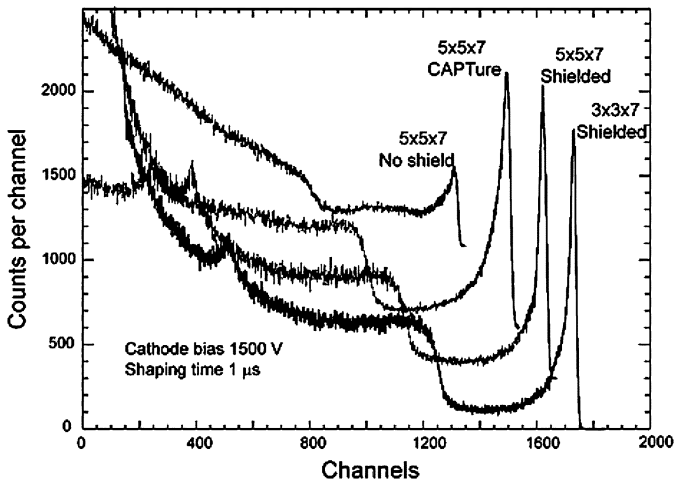

Fig. 3. Pulse-height spectra measured with different types of CZT devices fabricated of the same 7-mm thick crystal.

pogo-pin was used to apply a positive bias to the anode. In the second case, the anode was virtually grounded while negative bias was applied to the cathode. In addition, we had the option to apply any polarity bias to the side shield. Our preliminary measurements indicated no dependence of the device responses on the shield bias. Hence during the measurements, we normally connect the shield and cathode contacts to the same bias.

A standard ^{137}Cs radioactive source was used to observe the spectroscopic properties of the detectors. The signals were measured with eV Products 5092 preamplifier. The data acquisition system included a spectroscopy shaping amplifier, MCA card, digital oscilloscope to store waveforms readout from a charge-sensitive preamplifier, and standard NIM electronics.

There is a direct analogy between a virtual Frisch-grid device and a classic gas ionization chamber with a shielding grid actually located near the anode. The properly biased shielding grid provides 100% electron transmission and at the same time electrically shields the anode from any charges in the region between the cathode and grid (collection region). Charge induction upon the anode is mainly generated as the electrons travel in the space between the grid and the anode (induction region), whereas the grid screens charge induction from slow moving positive ions drifting toward the cathode. An important characteristic of the shielding grid is its shielding inefficiency [11], i.e., percentage of the field lines generated by a source charge located inside the collection region that penetrate through the grid. In other words, a small signal is induced even when the electron cloud drifts inside the collection region. In a semiconductor device, electrodes placed on the side surfaces create a virtual Frisch grid inside the crystal, thereby shielding charge carrier induction. As in the case of gas ionization chambers, the virtual grid is not 100% efficient. The shielding efficiency of the Frisch-ring device depends on the aspect ratio and fraction of the side surface area covered by the shielding electrode. In both types of detectors, the "poor" shielding or, using terminology applied to gas ionization chambers, the shielding inefficiency of the virtual Frisch grid, results in the degradation of the energy resolution.

III. Results and Discussions

The operational principle of the Frisch-ring detector is illustrated in Fig. 2, which shows the dependence of the induced charge on the anode versus the distance from the anode for different aspect ratios of the detector. To calculate this dependence, we modeled the Frisch-ring detector as a rectangular metal box with a square cross section of which one side (top or bottom) is the anode, while all the other sides (including the cathode) form the electrostatic shield. As shown in Fig. 2, for small aspect ratios, the majority of the charge is induced near the anode, which illustrates a formation of the virtual grid close to the anode. This is also illustrated in Fig. 3, which shows improvements in the device responses when detectors with smaller aspect ratios or larger fraction of shielded surface areas were used.

In agreement with other researchers [12], we have also observed significant variations in the pulse-height spectra with our Frisch-ring detectors fabricated as previously described. Moreover, detectors re-fabricated (re-polished or wrapped in a new copper shield) from the same material yielded varying results, which suggests that internal crystal defects cannot completely explain poor detector responses. Fig. 4 shows examples of pulse-height spectra measured with the detectors that had poor responses. The spectra were collected for two

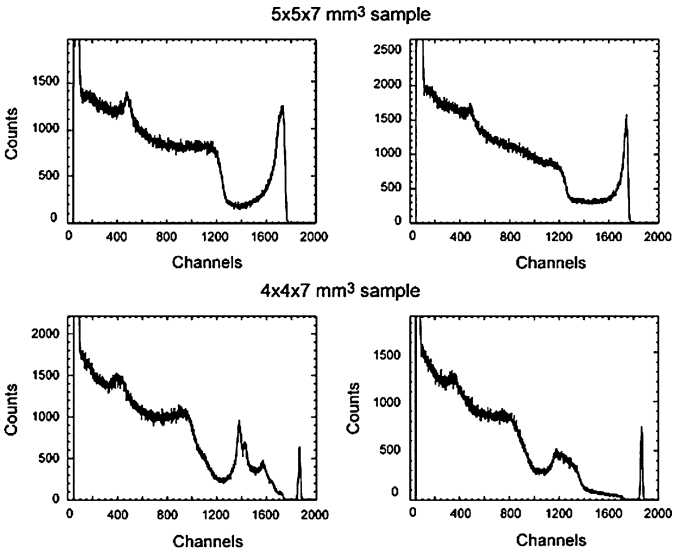

Fig. 4. Examples of pulse-height spectra measured with the detectors that had poor responses.

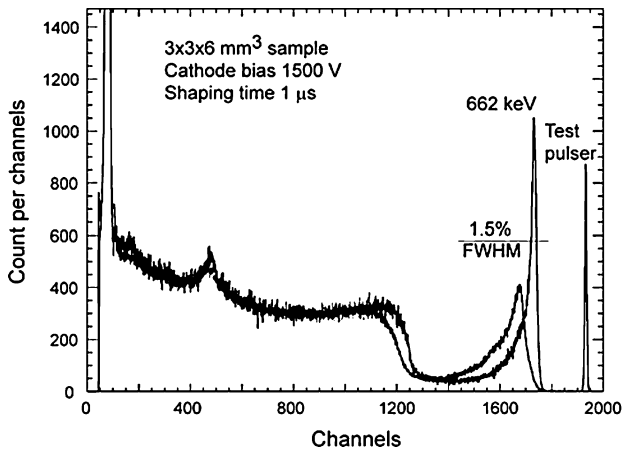

Fig. 5. Pulse-height spectra measured with the same device before and after surface passivation.

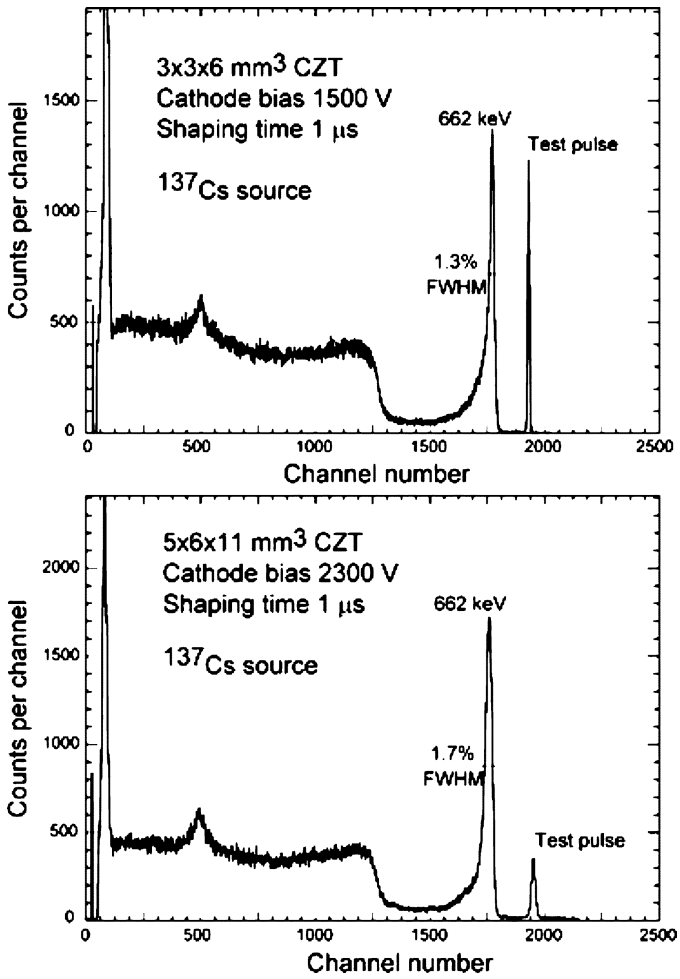

Fig. 6. Pulse-height spectra measured with "good" devices: $3 \times 3 \times 6$ mm^3 (top) and $5 \times 6 \times 11$ mm^3 (bottom).

orientations of a CZT crystal inside the detector's assembly (top and bottom sides were switched by placing the crystal up-side down). Generally, satellite peaks, strong tailing, and large low-energy background are very common features of the "bad" detectors. Furthermore, some detectors showed good responses. For good detectors a general tendency was observed that CZT detectors fabricated with the rougher lateral surfaces yielded better spectra, even though they had higher electronic noise and leakage current. This suggests that a certain level of surface leakage current is required to ensure a good detector performance. A possible explanation of this effect will be presented later.

Reliable surface control is difficult to achieve with simple mechanical polishing; a more reliable method would be to use a chemical process (surface passivation). We fabricated the best detectors by applying a chemical treatment in which highly polished crystals were submersed for several minutes in a NH_4F/H_2O_2 solution [10]. As an example, Fig. 5 shows two spectra measured with the same device before and after NH_4F/H_2O_2 treatment. Despite the observed improvement, the testing of a larger number of CZT samples is required before definite conclusion can be made regarding the best surface passivation.

Fig. 6 shows the pulse-height spectra measured with the $3 \times 3 \times 6$ and $5 \times 6 \times 11$ mm^3 devices with the best performance. By fitting the peaks with Gaussian curves we estimated energy resolutions of 1.3% and 1.7% FWHM at 662 keV, correspondingly. These are good results for such thick CZT detectors. The Compton continuum in the ^{137}Cs spectra is suppressed, as a result of placing the radioactive source upon the detector cathode. In contrast, the detectors with poor response usually show enhanced Compton continua in the low energy regions, most likely a consequence of low energy tailing from the full-energy peaks.

To better understand the cause of the poor detector responses, we measured and digitally analyzed the pulse shapes from the charge sensitive preamplifier. We found that the leading edge of the measured pulse-shapes generally has two slopes: a fast rising and slow rising part. The duration of the slow rising part can vary significantly. It can be very short and barely distinguished from the rounded top edge of a waveform due to the preamplifier rise-time. In the other extremes, it can be as long as several microseconds. For the majority of the events, the leading edges

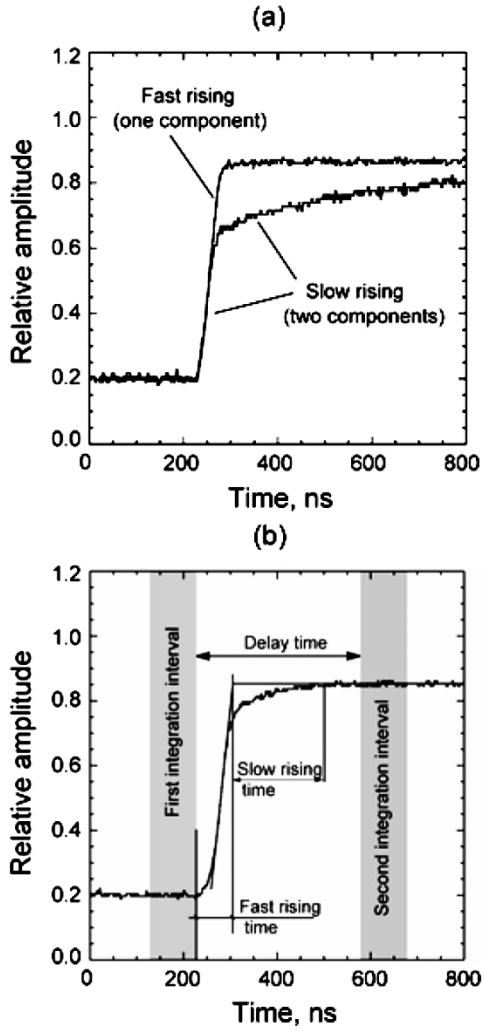

Fig. 7. Examples of measured waveforms. (a) Two extreme cases of slow and fast rising events. (b) Typical waveform with slow rising slopes.

of the waveforms have two parts with a clearly seen knee separating the fast and slow slopes. Examples of the fast and slow rising pulses are shown in Fig. 7(a), while Fig. 7(b) shows a more typical waveform.

Digital pulse processing was used to analyze the waveforms measured from the "good" and "bad" detectors. For every waveform comprised of 1024 points, the algorithm evaluated the rise times of the fast and slow portions of the signal as illustrated in Fig. 7(b). The fast rising time is the time interval between the beginning of the pulse and the moment corresponding to the intersection of two extrapolating lines: the first line extrapolates a fast leading edge (calculated by fitting a leading edge around the point corresponding to one half of the amplitude); the second line extrapolates the trailing edge of a waveform (calculated by fitting the last 500 points of the recorded waveform). The slow rise-time corresponds to the curved portion of the waveform that "smoothes" the corner between the fitted lines.

Based on the above definitions, it is clear that the fast rise-time represents an *expected* drift time of the electron cloud transiting from the point of interaction to the anode. Both the fast and slow rise times provide valuable information for understanding the device performance.

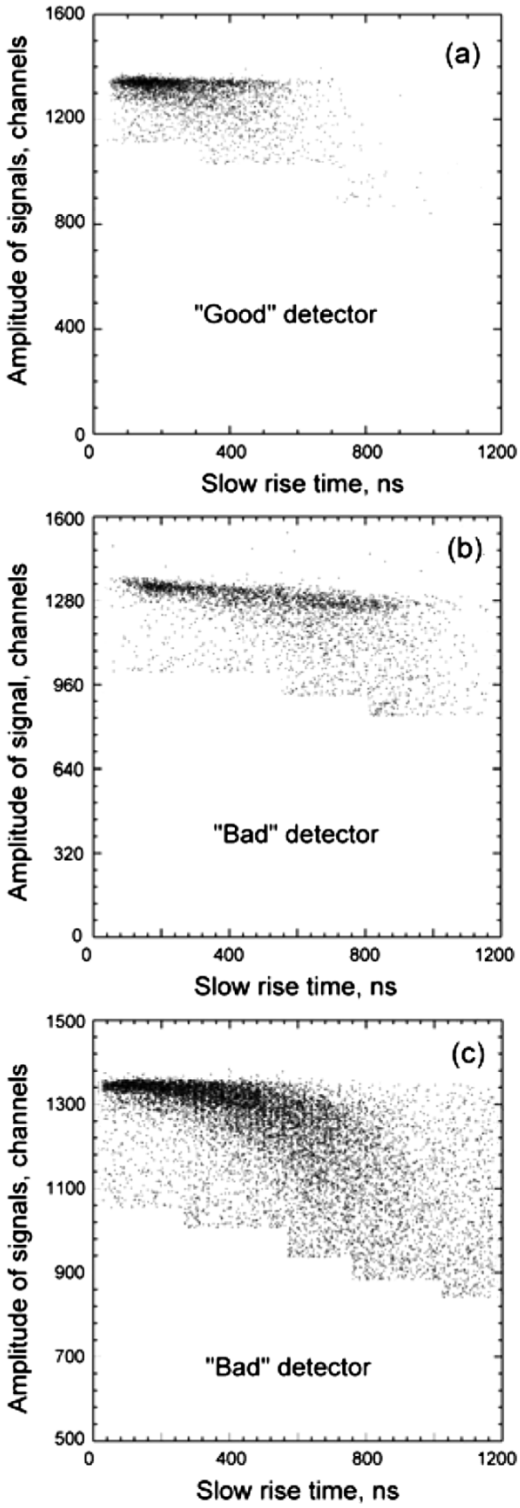

Fig. 8. Correlation between the amplitude of the signal and slow rise time evaluated for the "good" and "bad" detectors.

To evaluate the amplitude of the signals, the algorithm takes the difference between the base line and the pulse level as calculated by averaging the waveform data points over two 100 ns long time intervals (in the present case, these time intervals provide the optimal signal-to-noise ratio). To avoid the ballistic deficit a time delay up to 500 ns between the first and second integration windows was used.

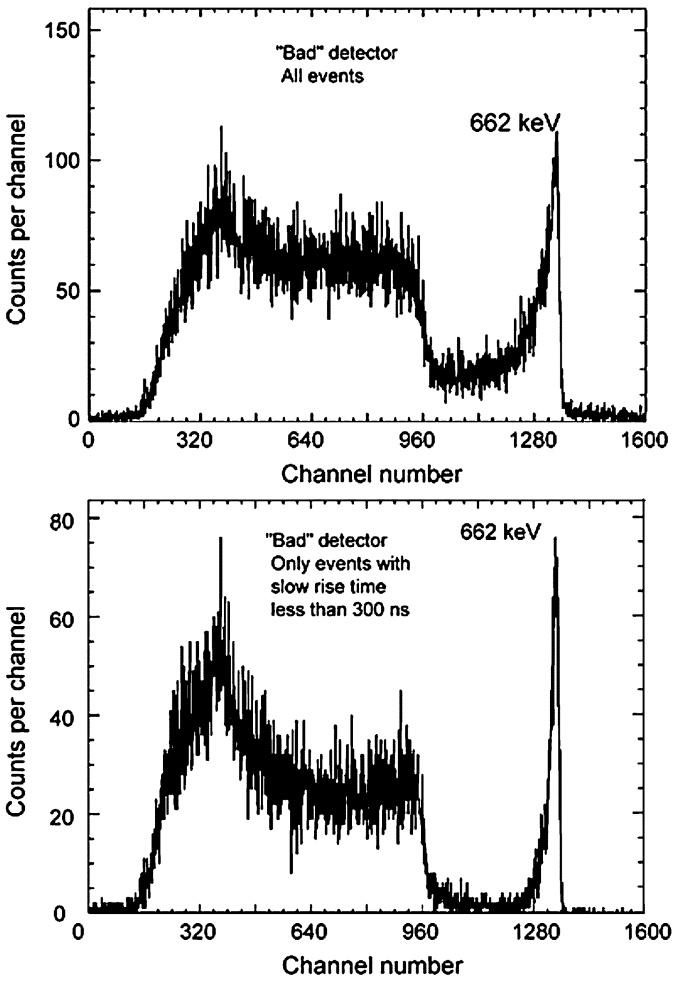

Fig. 9. Pulse-height spectra of ^{137}Cs measured for the "bad" detector: all events (top), events with slaw rise time less than 300 ns only (bottom).

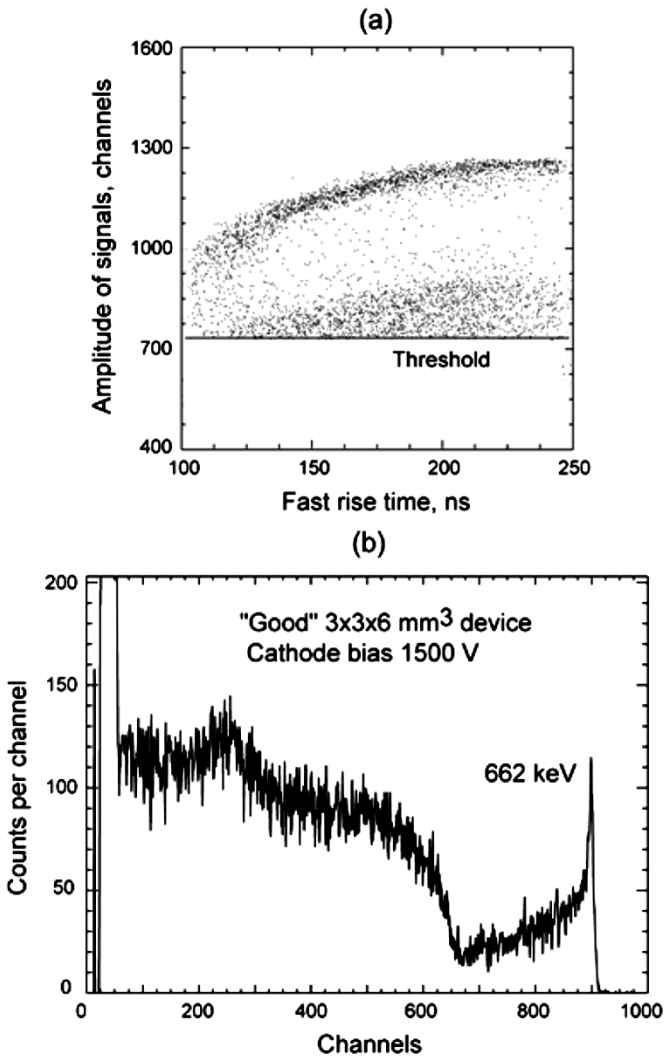

Fig. 10. Response of the "good" detector with a 2-mm-wide unshielded area of the side surfaces near the cathode. (b) A poor spectral response is due to (a) a strong depth dependence of the output signal amplitude .

A. Slow Rise Time

We observed that poor spectral response correlates with a large fraction $(> 50\%)$ of the events having leading edges with significantly long slow rising components (slow rising events). In contrast, the "good" detectors have more fast rising pulses with leading edges that are practically free of a slow rising component. Thus, the understanding of the origin of the "slow rising" events is a key to the fabrication of good virtual Frisch-grid detectors.

Shown in Fig. 8 is the correlation between the amplitude of the signals and slow rise time, with Fig. 8(a) and (b)–(c) exhibiting "good" and "bad" detectors, respectively. The detectors were irradiated with gamma rays from a ^{137}Cs source. While the "good" detector shows no correlation, the "bad" detector shows a correlation with the decay of the amplitude for the long rise times, which could be explained by the ballistic deficit effect. However, as is seen in Figs. 8(b) and (c), the track of the data points corresponding to the 662 keV peak shifts toward lower amplitudes as the slow rise time increases, which indicates that the "slow" events are associated with charge losses. This effect reduces the amplitude of the signals and introduces additional fluctuation in collected charge. Both the ballistic deficit and electron losses associated with slow rising events result in a poor spectral response of the detectors.

A notable improvement in the energy resolution can be achieved by rejecting the events with the slow rising times, e.g., above 300 ns, as shown in Fig. 9; however, this improvement is gained at the expense of the detection efficiency.

B. Fast Rise Time

As it was stated previously, the fast rise-time is an estimate of the expected drift time of the electron cloud transiting from the point of interaction to the anode. It also gives an estimate for the location of an interaction from the anode, which can be used to evaluate the device response versus the interaction depth. As an example, Fig. 10 illustrates a response of the "good" but insufficiently shielded detector that had a 2-mm-wide unshielded area of the side surfaces near the cathode. As shown, the poor spectral response [Fig. 10(b)] is due to a strong depth dependence of the output signal amplitude [Fig. 10(a)]. Fig. 11 illustrates the same effect but with a 1-mm unshielded area left near the anode. In this case, the copper provides better shielding efficiency. Both

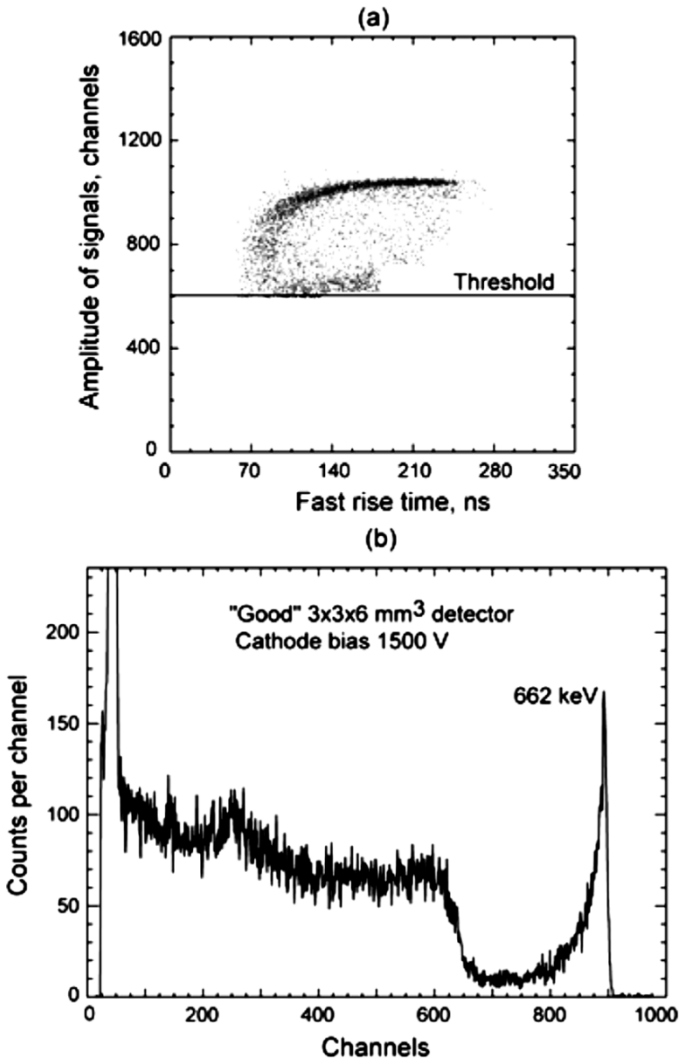

Fig. 11. Response of the "good" detector with a 1-mm-wide unshielded area of the side surfaces near the anode. (b) A poor spectral response is due to (a) a strong depth dependence of the output signal amplitude.

examples indicate the importance of shielding an entire area of the side surfaces of the device.

The low energy tails seen in the pulse-height spectra shown in Fig. 6 are due to the events interacting close to the anode where the shielding efficiency is poor. This is an intrinsic behavior of these types of devices: this region near the anode is a direct analog of the induction regain (between the grid and anode electrodes) in a gas ionization chamber. Fortunately, these events can be rejected by applying a rise time (or depth) selection which will have a very small impact on the photopeak efficiency [9].

C. Origin of Slow-Drift Regions

The slow rising part seen in the waveforms can be attributed to the electron cloud drifting inside the "low-drift-regions" located close to the anode. Alternatively, the collection of the holes could also generate the slow rising pulses, if the holes had a lifetime of several microseconds (same as duration of the slow rising events). However, in this case the detector response should be even better because of the hole contribution to the total

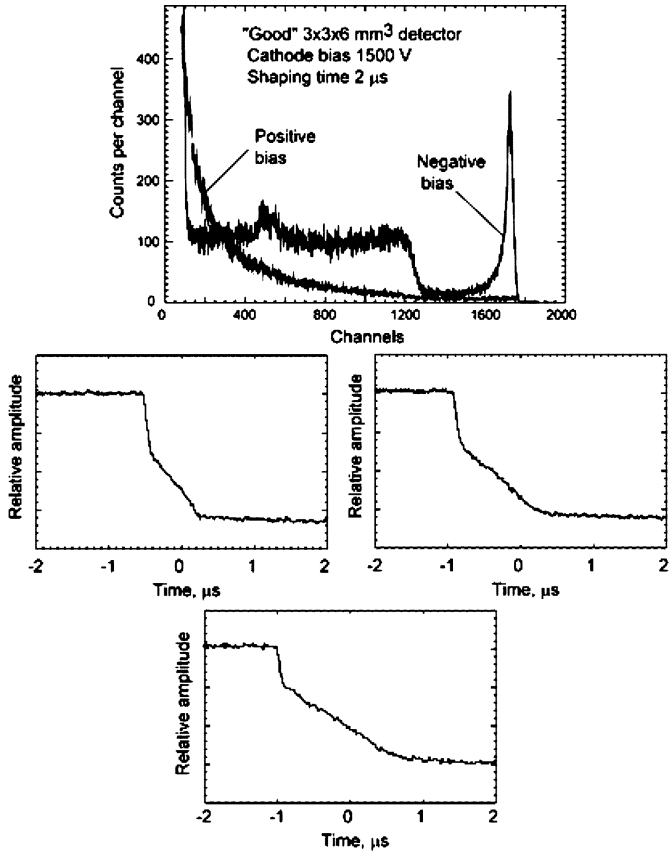

Fig. 12. Pulse-height spectra measured with the "good" detector for two polarities of the cathode bias: (a) positive versus negative and (b) abnormal slow rising pulses measured at the positive cathode bias.

collected charge. But in reality, as we observed, a poor detector response always correlates with the slow rising events. Moreover, if the hole lifetime were several microseconds, we would expect to see a reasonably good pulse-height spectrum induced by the holes when a positive (instead of the negative) bias is applied to the cathode and shield. Fig. 12 shows the pulse-height spectra measured with a "good" detector when positive and negative biases are applied to the cathode and shield. No peak indications are seen in the pulse-height spectrum collected at the positive bias, while the good spectrum is measured at the negative bias, which indicates a very poor hole collection efficiency.

As we took the measurements with the positively biased "good" detector, we surprisingly observed the same two-slope long-rising events that we saw with the negatively biased "bad" detectors. Based on these two facts we concluded: (1) the slow rising events are indeed generated by the electron cloud moving inside the slow-drift-regions, which can be identified simply as the device's side surfaces, and (2) the difference between the "good" and "bad" detectors can be explained by the different electric field lines distributions inside the devices. In a negatively biased "good" device the electric field lines are focused toward the anode and, as a result, electrons are steered away from the side surfaces. When the polarity is changed, the electric field becomes defocusing. Electrons drift toward the side surfaces and then continue to drift along the surface where the drift velocity is smaller than in the bulk due to electron scattering from the surface. This generates the two-slope rising

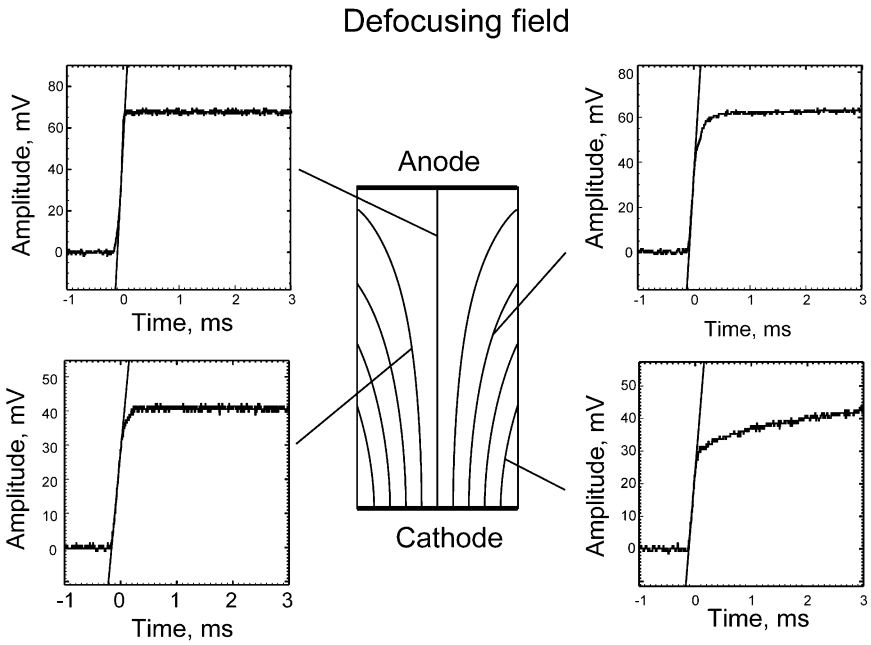

Fig. 13. Defocusing electric field resulting in slow-rising events.

signals. In the case of the "bad" detector, of course, everything is reversed.

The electric field distribution inside the Frisch-ring detector is determined by the boundary conditions (potential distribution) on the device side surfaces, which is mainly determined by the surface properties and the nature of the surface leakage current. These two factors control the surface charge and electrostatic potential distributions along the surface. The effects related to the surface leakage current in CZT devices were investigated in the past [13]–[15]. Despite the fact that most of the measurements were carried out for the narrow gaps between the contacts (in comparison to the electrodes size and device thickness) some results can be applicable to the Frisch-ring detectors. One of them is that the electrostatic potential on CZT surface depends on the CZT surface treatment. For more details, we refer to the results described in the above mentioned articles. From the general point of view, depending on the surface potential distributions there could be three outcomes for the electric field distribution inside the device as illustrated in Fig. 13. If the surface potential decreases (in absolute values) faster than linear function from the cathode level toward the anode a defocusing field is generated inside the device from which a poor response would be expected.

This interpretation is also supported by the measurements of the uniformity of the detector response with a highly collimated x-ray beam. The measurements were taken at National Synchrotron Light Source at Brookhaven National Laboratory. The beam size was 25×25 μm, and the energy of photons was $\sim$75 keV. For each x-ray beam position a pulse-height spectrum was collected, and the centroid position of the peak was evaluated. Fig. 14 shows the distribution of the peak position over the cathode area measured for the "bad" $4 \times 4 \times 6$ mm^3 (100-μm step size) and "good" $3 \times 4 \times 6$ (50-μm step size) Frisch-ring devices. As can be seen, the "bad" detector has very nonuniform response with significant loss in signal amplitudes near the detector edges.

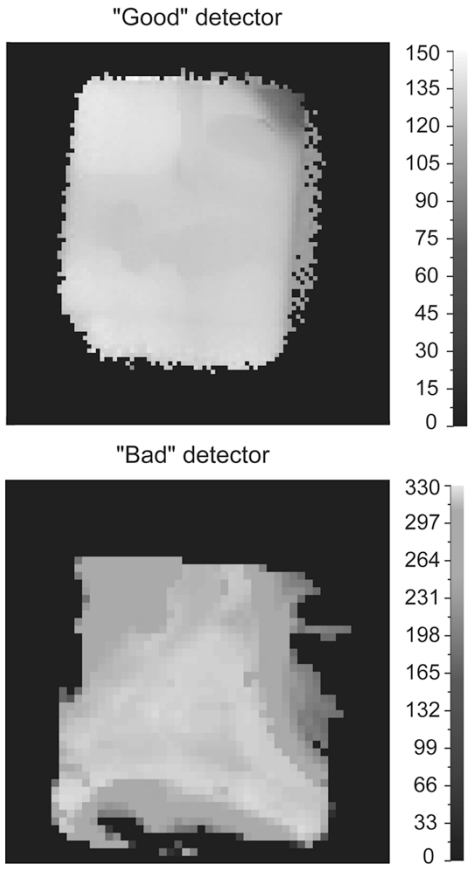

Fig. 14. Two-dimensional distribution of the peak position over the cathode area measured for the "bad" and "good" Frisch-ring devices.

IV. Conclusion

The Frisch-ring detector has a simple design and operates as a single-carrier device. Despite the simplicity of this device, its performance depends on the balanced combinations of several factors.

One of the critical factors is the electric field distribution inside the detector, which correlates with the CZT surface treatment. It was observed that a poor detector response can be attributed to a large fraction of the events that generate the slow rising component of pulses with leading edges that have two slopes: fast and slow. The fast rising part corresponds to the electron cloud transiting from the point of interaction to the anode. The slow rising part may be an indication that the electrons drift on the side surfaces of the device where the electron drift velocity is very low in comparison to those in the bulk. Such situation may arise because of the defocusing effect of the electric field inside the detector. That is, a fraction of the electric field lines intersect the detector surfaces instead of extending to the anode. A defocusing electric field would cause the electrons to drift to the near surface layer with electronic properties different from the bulk of CZT, which include lower mobility, higher trap concentration, etc. Slow rising events contribute to poor device response in two ways: (1) ballistic deficit and (2) the slow drifting electrons have higher probability to become trapped.

The second important factor is the shielding inefficiency of the Frisch-ring device. Effectiveness of the shielding electrode depends on the detector aspect ratio, thickness of the insulating layer between the shield and CZT surface, and a fraction of the side surface area covered by the shield. We fabricated good detectors with the aspect ratio 0.5 or less when the shield covered the entire area of the side surfaces of the device.

Acknowledgment

The authors would like to thank G. De Geronimo, D. P. Siddons, P. O'Connor, and G. Smith for help and fruitful discussions.

References

[1] T. E. Schlesinger and R. B. James, "Semiconductors and semimetals," in *Semiconductors for Room Temperature Nuclear Detector Applications*. San Diego, CA: Academic, 1995, vol. 43.

[2] G. F. Knoll, *Radiation Detection and Measurement*, 3rd ed. New York: Wiley, 2000.

[3] O. Frisch, "British Atomic Energy Report,", 1944. BR-149.

[4] D. S. McGregor, Z. He, H. A. Seifert, D. K. Wehe, and R. A. Rojeski, "Single charge carrier type sensing with a parallel strip pseudo-frisch-grid CdZnTe semiconductor radiation detector," *Appl. Phys. Lett.*, vol. 72, pp. 792–794, 1998.

[5] D. S. McGregor and R. A. Rojeski, "High-resolution ionization detector and array of such detectors," U.S. Patent 6 175 120, Jan. 6, 2001.

[6] D. S. McGregor, "Collimated radiation detector assembly, array of collimated radiation detectors and collimated radiation detector module," U.S. Patent 2003-0 034 456, Feb. 20, 2003.

[7] G. Montémont, M. Arques, L. Verger, and J. Rustique, "A capacitive frisch grid structure for CdZnTe detectors," *IEEE Trans. Nucl. Sci.*, vol. 48, no. 3, pp. 278–281, Jun. 2001.

[8] W. J. McNeil, D. S. McGregor, A. E. Bolotnikov, G. W. Wright, and R. B. James, "Single-charge-carrier-type sensing with an insulated frisch ring CdZnTe semiconductor radiation detector," *Appl. Phys. Lett.*, vol. 84, pp. 1988–1990, 2004.

[9] A. E. Bolotnikov, G. S. Camarda, G. A. Carini, G. W. Wright, D. S. McGregor, W. McNeil, and R. B. James, "New results from performance studies of frisch-grid CdZnTe detectors," *Proc. SPIE*, vol. 5540, pp. 33–45, 2004.

[10] G. W. Wright, G. Camarda, E. Kakuno, L. Li, F. Lu, C. Lee, A. Burger, J. Trombka, P. Siddons, and R. B. James, "Effects of surface roughness on large-volume CdZnTe nuclear radiation detectors and removal of surface damage by chemical etching," *Proc. SPIE*, vol. 5198, pp. 306–313, 2004.

[11] O. Buneman, T. E. Cranshaw, and J. A. Harvey, "Design of grid ionization chambers," *Can. J. Res.*, vol. A27, pp. 191–206, 1949.

[12] L. Cirignano, H. Kim, K. Shah, M. Klugerman, P. Wong, M. Squillante, and L. Li, "Evaluation of CZT detectors with capacitive frisch grid structure," *Proc. SPIE*, vol. 5198, pp. 1–8, 2004.

[13] A. E. Bolotnikov, S. E. Boggs, C. M. H. Chen, W. R. Cook, F. A. Harrison, and S. M. Schindler, "Properties of Pt Schottky type contacts on high-resistivity CdZnTe detectors," *Nucl. Instrum. Meth.*, vol. A482, pp. 395–407, 2002.

[14] A. E. Bolotnikov, C. M. H. Chen, W. R. Cook, F. A. Harrison, I. Kuvvetli, S. M. Schindler, C. M. Stahle, and B. H. Parker, "The effect of cathode bias (field effect) on the surface leakage current of CdZnTe detectors," *Nucl. Instrum. Meth.*, vol. A510, pp. 300–308, 2003.

[15] A. E. Bolotnikov, C. M. H. Chen, W. R. Cook, F. A. Harrison, I. Kuvvetli, and S. M. Schindler, "Effects of bulk and surface conductivity on the performance of CdZnTe pixel detectors," *IEEE Trans. Nucl. Sci.*, vol. 49, no. 4, pp. 1941–1949, Aug. 2002.